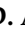




## Article

# Enhanced Oil Spill Remediation Using Environmentally Asymmetric Dicationic Ionic Liquids: Synthesis, Characterization, and Evaluation

Rima D. Alharthy <sup>1</sup>, C. E. El Shafiee <sup>2,3</sup>, M. I. Nessim <sup>2</sup>, R. I. Abdallah <sup>2,3</sup>, Y. M. Moustafa <sup>2</sup>, M. Wafeek <sup>4</sup>, D. A. Ismail <sup>5</sup>, M. M. H. Khalil <sup>6</sup> and R. A. El-Nagar <sup>2,3,\*</sup>

<sup>1</sup> Department of Chemistry, Science & Arts College, Rabigh Branch, King Abdulaziz University, Rabigh 21911, Saudi Arabia; [iaaalharte@kau.edu.sa](mailto:iaaalharte@kau.edu.sa)

<sup>2</sup> Analysis and Evaluation Department, Egyptian Petroleum Research Institute, Nasr City, Cairo 11727, Egypt

<sup>3</sup> Routine Lab, Central Lab, Egyptian Petroleum Research Institute, Nasr City, Cairo 11727, Egypt

<sup>4</sup> Aquaculture Research Center, Ismailia Governorate 8314024, Egypt

<sup>5</sup> Petrochemical Department, Egyptian Petroleum Research Institute, Nasr City, Cairo 11727, Egypt

<sup>6</sup> Faculty of Science, Ain Shams University, Cairo 11566, Egypt

\* Correspondence: [raghda\\_elnagar@yahoo.com](mailto:raghda_elnagar@yahoo.com)

**Abstract:** The disastrous consequences for society—economically, environmentally, and socially—caused by oil spills encouraged us to treat this problem. The target of this work is to synthesize new amphiphilic dicationic ionic liquids (Ia, Ib, and Ic) and evaluate them spectroscopically and gravimetrically as potential oil spill dispersants at different temperatures to cover cold and warm areas. The synthesized ILs were well characterized by different tools for analysis of their surface activity and thermal stability. Ia, Ib, and Ic showed good dispersion effects, which were recorded to be 5.32, 20.45, and 33.61% for Ia, Ib, and Ic, respectively, at 10 °C and 12.28, 52.55, and 66.80% for Ia, Ib, and Ic, respectively, at 30 °C with a dispersant-to-oil ratio (DOR) of 0.8:10 (wt.%). Acute toxicity tests were elucidated against Nile tilapia and *Oreochromis niloticus* fish and confirmed their slight toxicity by determining a LC50 value greater than 100 ppm after 96 h, which recorded 13.25, 17.75, and 37.5 mg/L for Ia, Ib, and Ic, respectively. Overall, the new synthesized ILs can be represented as sustainable materials for toxic chemicals to disperse oil spills.

**Keywords:** ionic liquids (ILs); amphiphilic; asphaltene dispersion; oil spill; acute toxicity test



**Citation:** Alharthy, R.D.; El Shafiee, C.E.; Nessim, M.I.; Abdallah, R.I.; Moustafa, Y.M.; Wafeek, M.; Ismail, D.A.; Khalil, M.M.H.; El-Nagar, R.A. Enhanced Oil Spill Remediation Using Environmentally Asymmetric Dicationic Ionic Liquids: Synthesis, Characterization, and Evaluation. *Separations* **2023**, *10*, 397. <https://doi.org/10.3390/separations10070397>

Academic Editor: Sascha Nowak

Received: 7 February 2023

Revised: 26 April 2023

Accepted: 25 May 2023

Published: 10 July 2023



**Copyright:** © 2023 by the authors. Licensee MDPI, Basel, Switzerland. This article is an open access article distributed under the terms and conditions of the Creative Commons Attribution (CC BY) license (<https://creativecommons.org/licenses/by/4.0/>).

## 1. Introduction

Oil spills are a type of pollution that is released from petroleum hydrocarbons into the surrounding environment [1], especially the marine eco-system, as a result of enormous human activities [2]. Oil spills can cause severe negative effects economically [3,4], environmentally, and socially [5,6]. Consequently, accidents spark a lot of political and media interest [7], which makes the government and the political community struggle together to respond to the oil spill and take the appropriate action to protect the environment from serious disaster [8,9].

The current challenge is to clean up oil spills caused by accidents. Accidents involving oil spills will continue to occur because society relies heavily on various petroleum products [10]. Oil spill treatment methods can be classified as mechanical, biological, or chemical. In mechanical treatment, skimmers are fixed or mobile devices used for the removal of floating and/or emulsified oil from the surface of the water [11]. Biological treatment includes the addition of microbes, nutrients, and/or oxygen and the subsequent biodegradation of spilled oil [12]. A diverse community of microorganisms is being formed that can use them as their sole carbon source to degrade petroleum hydrocarbons. Chemical treatments include dispersants sprayed on oil spills to break them up into small droplets.

The oil dispersants split the oil slicks by minimizing the oil–water interface and accelerating the breakdown of the hydrophobic oil portion.

The use of IL-based surfactants for oil spill remediation is a relatively novel strategy [13,14]. Due to their prospective environmental and technological advantages of low volatility, low toxicity, high surface activity [15], and thermal stability [16], ILs have garnered a lot of attention [17]. A new class of dicationic ionic liquids (DILs) has been introduced. DILs are more adaptable than monocationic ionic liquids (MILs). That is referring to the enormous possible changes in the molecular structure by changing the cation or anion type; furthermore, the side chain linker between the two head groups could be a rigid or flexible spacer [16].

Usually, DILs exhibit greater thermal stability compared with MILs. They display decomposition temperatures between 330 and 400 °C and 145 and 185 °C for DILs and MILs, respectively. DILs are more viscous than MILs [17], so they have a wide range of applications, including high-temperature lubrication, as catalysts in esterification reactions, asphaltene, and oil spill dispersion [14].

The amphiphilic surface-active ILs showed perfect surface activity with self-assembling characteristics [18]. However, the rising concerns about the traditional ILs' toxicity restricted their usage as oil dispersants and established the importance of biocompatibility and biodegradability for their effective and environmentally sustainable use [19,20]. Baharuddin et al. prepared 1-butyl-3-methylimidazolium lauroylsarcosinate, 1,1'-(1,4-butanediyl)bis(1-*H*-pyrrolidinium) dodecylbenzenesulfonate, tetrabutylammonium citrate, tetrabutylammonium polyphosphate, tetrabutylammonium ethoxylate, and oleyl ether glycolate, which results in their classification as partially non-toxic.

From this point on, the target of this study was to provide new insight for environmentally developed ILs as oil dispersants to replace the current hazardous chemical dispersants. Three different ILs, namely, 1-(6-(1-dodecyl-2-methyl-1*H*-imidazol-3-ium-3-yl) hexyl) pyridin-1-ium bromide (Ia), 1-(6-(1-dodecyl-2-methyl-1*H*-imidazol-3-ium-3-yl) hexyl)-3-methylpyridin-1-ium bromide (Ib), and 1-(6-(1-dodecyl-2-methyl-1*H*-imidazol-3-ium-3-yl) hexyl)-4-methyl pyridin-1-ium bromide (Ic) were synthesized, well characterized and lab scale examined as oil dispersants.

## 2. Methodology

### 2.1. Materials and Characterizations

The chemicals and reagents used were of analytical grade, supplied by Merck, and were used directly without previous purifications. 1-bromodecane ( $\geq 98\%$ ), 2-methylimidazole ( $\geq 99\%$ ), pyridine ( $\geq 98\%$ ), and potassium hydroxide ( $\geq 97\%$ ) 3-Methylpyridine ( $\geq 99\%$ ), 4-methylpyridine ( $\geq 99\%$ ), acetonitrile ( $\geq 97\%$ ), 1,6-dibromohexane ( $\geq 99\%$ ), ethyl acetate ( $\geq 98\%$ ), hexane ( $\geq 99\%$ ), benzene ( $\geq 97\%$ ), aluminum oxide (neutral), silica gel, filter paper Whatman No. 1, and chloroform ( $\geq 99\%$ ). Heavy crude oil, delivered from West Bakr Petroleum Company, has physicochemical characteristics (according to standard test methods) as shown in Table 1. Sea water (the Red Sea) was characterized in Tables 2 and 3.

The FT-IR bands of the prepared compounds were examined using a Nicolet Ia-10 at scan resolutions of 4000–400  $\text{cm}^{-1}$  and 4  $\text{cm}$  and a scan rate of 32  $\text{cm}/\text{min}$ , in that order.  $^1\text{H-NMR}$  spectra were screened using BURKER  $^1\text{H-NMR}$  spectroscopy in DMSO- $d_6$  solvent. (400.19 MHz and a 5-mm broad-band inverse Z gradient probe). Elemental analysis was achieved via an elemental analyzer. Thermogravimetric analysis was studied using a thermal analyzer at a heating rate of 10 °C/min. Samples are heated from ambient temperature up to 600 °C under nitrogen flow. The thermal degradation discussion was revealed at the point of 95% weight loss from the original weight. Surface tension parameters were obtained by a tensiometer (Du Nouty) with a platinum ring. Fresh aqueous solutions of the examined ILs (as surfactants) were prepared and measured within 0.01–0.00001 M/L at the 25 °C concentration range.

**Table 1.** Physicochemical characterization of heavy crude oil [21].

Experiment	Method	Result
Density@ 15.56 °C		0.9558
Specific gravity API	ASTM D-4052	0.9568 16.3
Kinematic Viscosity @40 °C, cSt	ASTM D-445	1820.35
Wax content, wt. %	UOP-64	1.37
Water content, vol. %	ASTM D-4006	7.5
Pour point, °C	ASTM D-97	15
Flash point, °C	ASTM D-93	<−22
Group composition (SARA Analysis)		
Saturates		18.18
Aromatics		37.99
Resin		30.24
Asphaltene	IP-143	13.59

**Table 2.** Physical characteristics of sea water.

<b>Total Dissolved Solids (T.D.S.)</b>	46,191.9 mg/L	<b>Density @ 60 F</b>	1.03207 g/mL
<b>Salinity (as NaCl)</b>	45,568.1 mg/L	<b>Specific gravity</b>	1.03310
<b>Alkalinity (as CaCO<sub>3</sub>)</b>	150.1 mg/L	<b>pH @ 25 °C</b>	7.8
<b>Total Hardness (as CaCO<sub>3</sub>)</b>	8760.1 mg/L	<b>Conductivity</b>	$6.46 \times 10^{-2}$ mhos/cm @17.8 °C
		<b>Resistivity</b>	0.1548Ohm-m @17.8 °C

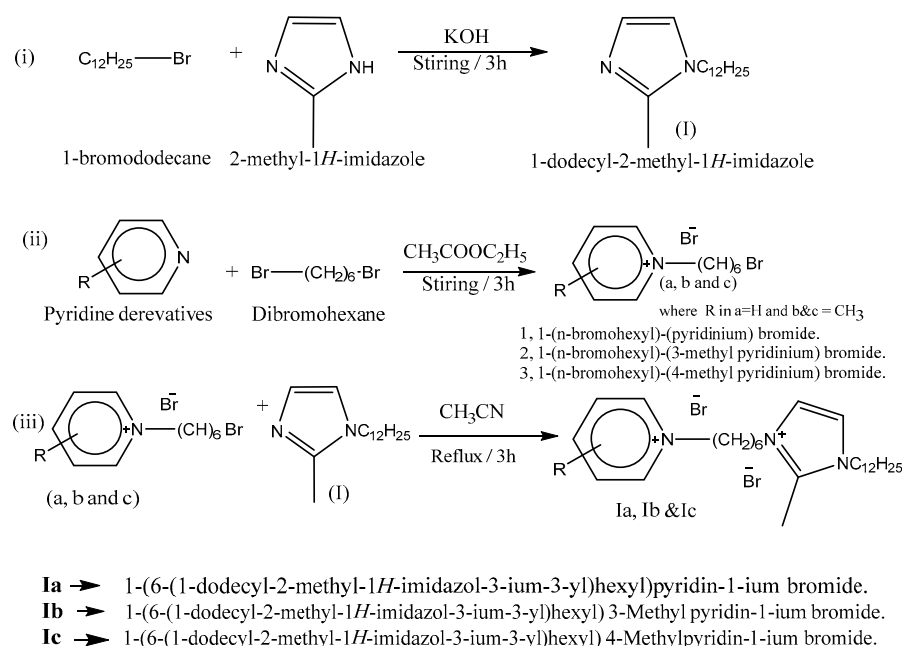
**Table 3.** Inorganic Chemical Constituents of sea water.

Cation	mg/L	meq/L	Anion	mg/L	meq/L
Lithium	4.21	0.607	Fluoride	0.50	0.026
Sodium	14,132.00	614.459	Chloride	27,617.00	777.971
Ammonium	<0.0005	<0.00001	Bromide	40.00	0.501
Potassium	507.12	12.972	Nitrate	<5	<0.2
Magnesium	1654.30	136.133	Nitrite	111.00	2.408
Calcium	779.99	38.921	Phosphate	<0.07	<0.0022
Strontium	58.37	1.332	Sulfate	1032.00	21.497
Barium	72.37	1.054	Hydroxide	$>1.81 \times 10^{-7}$	$>2 \times 10^{-8}$
Iron	>0.5	>0.018	Carbonate	>100	>3.27
Copper	>0.001	$>3.17 \times 10^{-5}$	Bicarbonate	183.00	2.999

## 2.2. Synthesis of Amphiphilic Asymmetric Dicationic Ionic Liquids

- i. Compound I was previously prepared in our previous work [20,21] by stirring 0.1 mL of 2-methyl imidazole with potassium hydroxide dissolved in acetonitrile. Following the addition of 0.1 of bromododecane, which was completely miscible, drop by drop, the stirring stopped when the white precipitate was noticed (after about 3 h). By filtration, the white precipitate of KBr was eliminated, and the filtrate was vaporized in an oven under vacuum.
- ii. a, b, and c were prepared by mixing pyridine, 3-methylpyridine, or 4-methylpyridine (0.1 mol) with 0.1 mol of 1,6-dibromohexane for 3 h at ambient temperature. [22]. Ia, Ib, and Ic (dicationic ILs) were synthesized by the compounding of compound I (1:1) with a, b, and c under refluxing for 3 h. The products were collected and dried via evaporation under vacuum (89.2, 87.5, and 89.4% yield).

The completion of the reaction was monitored and confirmed by the TLC technique in Scheme 1.



Scheme 1. Synthesis of Ia, Ib & Ic.

### 2.3. Quantum Chemical Parameters

Synthesized ionic liquids (Ia, Ib, and Ic) differ from each other by the type of cation. Quantum chemical calculations and the geometric shape of prepared molecules were performed using density functional theory (DFT). The quantum chemical calculations were performed by utilizing the basis set 6-31G'(d,p), where Beck's three-parameter exchange functional was used along with the Lee-Yang-Parr nonlocal correlation function (B3LYP). The highest occupied molecular orbital (HOMO) and lowest unoccupied molecular orbital (LUMO) were studied for all synthesized compounds. The calculated quantum parameters, including energy gap ( $\Delta E$ ), chemical hardness ( $\eta$ ), chemical softness ( $\sigma$ ), dipole moment ( $\mu$ ), and electron affinity (A), were recorded. Chemical hardness ( $\eta$ ) is defined as the resistance of an atom to the transfer of charge or change in its electron configuration and is estimated according to Equation (1).

$$\eta = -1/2 (E_{HOMO} - E_{LUMO}) \quad (1)$$

The softness ( $\sigma$ ), which is described as the capacity of the atom or atom group to receive electrons, can be estimated according to Equation (2).

$$\sigma = 1/\eta = -2 (E_{HOMO} - E_{LUMO}) \quad (2)$$

The ionization potential (I) can be derived from  $E_{HOMO}$ , while the electron affinity (A) related to  $E_{LUMO}$ .

$$I = E_{HOMO} \quad (3)$$

$$A = E_{LUMO} \quad (4)$$

### 2.4. Evaluation of the Prepared ILs for Oil Spill Remediation

#### Efficiency Test

The competence of Ia, Ib, and Ic as oil dispersants at different temperatures and concentrations was illustrated using the same method as discussed in our previous work [21]. Figure 1 shows how 250 mL of seawater was poured into a separate funnel that was kept

at a constant temperature, and then 5 mL of crude oil was added to the water surface for 1 min. The amounts of different concentrations of the studied dispersants were determined, the water with oil and dispersant was shaken, 50 mL of oily water emulsion was taken in a measuring cylinder, and finally the oil was extracted using chloroform. The extracted oil in chloroform was transferred into a 100 mL volumetric flask, completed with chloroform to the mark, and mixed well. By using UV spectroscopy, determine the absorption of the extract against the blank. The efficiency index was calculated according to the following Equation (5):

$$E\% = \frac{\text{Weight of oil in 50 mL sample of oily water} \times 500}{\text{weight of added oil}} \quad (5)$$

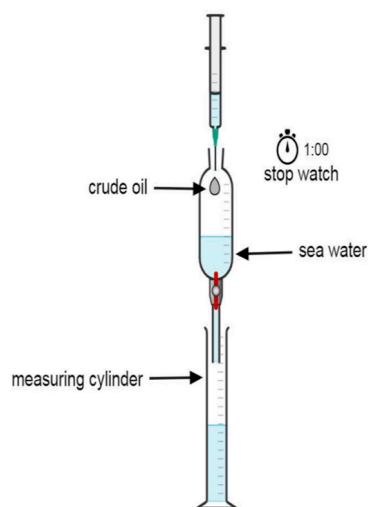


**Figure 1.** Efficiency test.

The treated crude oil was studied by SARA analysis (saturates, aromatics, resin, and asphaltene), where asphaltene content must be determined and isolated. The asphaltene utilized in our study was extracted from West Bakr Petroleum Company's heavy crude oil according to IP-143 (the standard method). A specific amount (10 g) of the crude oil was refluxed for 1 h with 300 mL of n-heptane. Allow the mixture to cool for 2 h in a dark place before filtering. Inorganic materials, waxy substances, and asphaltene were still on the filter paper, which was folded and placed in soxhelt to be washed with heated n-heptane to get rid of any waxy substances. The asphaltene was dissolved in hot toluene. Finally, evaporate the toluene and calculate the asphaltene percent according to the following Equation (6):

$$A = 100 \times \frac{M}{G} \quad (6)$$

where  $M$  and  $G$  refer to the mass of asphaltene and crude oil in grams, respectively.

Maltene, or deasphalted oil, is then separated into saturates, aromatics, and resins according to ASTM D 2007. Saturates and aromatics were analyzed by GC and HPLC spectroscopy. The saturates were analyzed by a gas chromatography mass spectrometer (GC-MS, QP 2010) using a DB-5 capillary column (containing 5% phenyl and 95% polydimethyl siloxane) and measured at  $30 \text{ m} \times 0.32 \text{ mm} \times 0.23 \text{ }\mu\text{m}$  film thickness. The MS scan parameters were an  $m/z$  range of 40–500, a scan interval of 0.5 s, a scan speed of  $1000 \text{ amu s}^{-1}$  and a detector voltage of 1.1 kV. It is the used carrier gas, and with a constant linear velocity of  $1.1 \text{ mL min}^{-1}$  and a programmed temperature (of 40–280 °C at  $2 \text{ }^\circ\text{C min}^{-1}$ ) the samples were held for 30 min at 280 °C.

Aromatics were analyzed to detect PAHs by HPLC (Agilent Technologies 1200 Series HPLC) with a UV detector using a ZORBAX 5  $\mu\text{m}$ ,  $4.6 \times 250 \text{ mm}$   $\text{NH}_2$ -column, which separates the aromatic fractions into sub-fractions. N-heptane was used as the mobile

phase in a column with a flow rate of 3 mL/min. The delay and elution time were detected, and the aromatic sub-fractions were noticed in the HPLC figures. All the HPLC systems were kept at room temperature, and the data handling was justified by Agilent software (Santa Clara, CA, USA) [23].

### 2.5. Acute Toxicity Test

The compounds (Ia, Ib, and Ic) were tested against healthy Nile tilapia, *Oreochromis niloticus*, with an average body weight of  $40.0 \pm 2.0$  g. Each treatment had three replicates for each compound. The lab conditions have to stay constant. Abnormal behavior and dead fish were noticed and recorded every day for four days. Then the value of the 96 h LC50 was calculated [24].

Determination of the 96-h LC50 = Biggest concentration -  $\Sigma ab/n$ .

## 3. Results and Discussions

### 3.1. Characterization of the Synthesized ILs

FT-IR spectrum Figure 2 revealed that N-H broad stretching peaks appeared around  $3416\text{--}3439\text{ cm}^{-1}$ . The stretching peaks in the range  $3017\text{--}3050\text{ cm}^{-1}$  were resorted to by C-H aromatic stretching, which belongs to the vibrational motion in the imidazole ring [25], while the aliphatic stretching asymmetric C-H appeared between  $2853$  and  $2922\text{ cm}^{-1}$ . C-C vibrations related to the imidazole ring were recorded between  $1631$  and  $1642\text{ cm}^{-1}$ . The peaks between  $1375$  and  $1380\text{ cm}^{-1}$  resorted to the C-N bending symmetrical mode of vibrations in imidazole rings. The vibrational bending (in plane) peaks of imidazole appeared around  $1152\text{--}1183\text{ cm}^{-1}$ . While the values  $725\text{--}773\text{ cm}^{-1}$  are attributed to the out-of-plane bending vibrations.

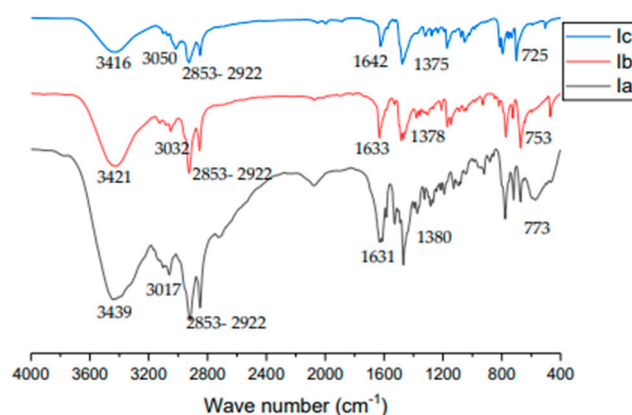


Figure 2. FT-IR of Ia, Ib & Ic.

$^1\text{H-NMR}$  spectrum for Ia, Ib, and Ic were confirmed and detected, as shown in Figures 3–5 and Tables 4–6.

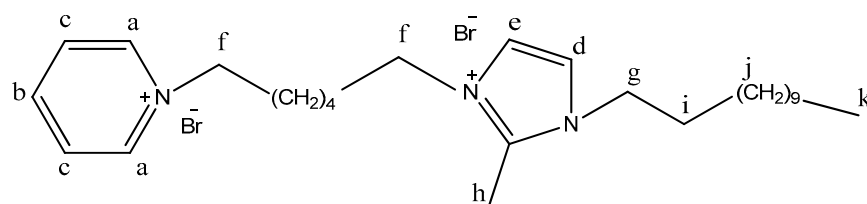


Figure 3. Chemical structure of Ia.

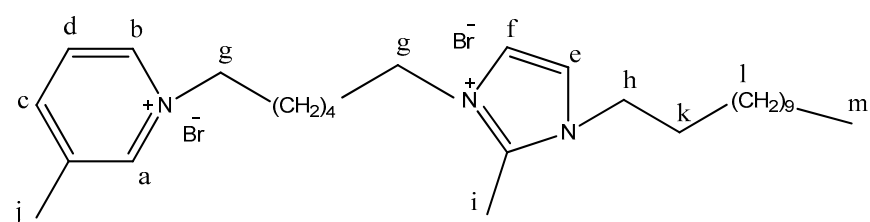


Figure 4. Chemical structure of Ib.

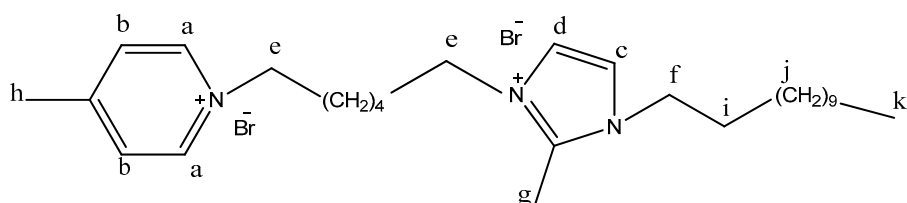


Figure 5. Chemical structure of Ic.

Table 4. <sup>1</sup>H-NMR protons for Ia.

Comp	A (d)	B (t)	C (t)	d (d)	e (d)	F (t)		g (t)	h (s)	i (m)	J (s)	K (t)
Ia	9.22	8.63	8.10	7.78	7.24	$\frac{f_1}{4.32}$	$\frac{f_2}{3.98}$	3.98	3.63	2.54	1.19	0.84

Table 5. <sup>1</sup>H-NMR protons for Ib.

Comp	a (s)	b (d)	C (d)	d (t)	e (d)	f (d)	g (t)		h (t)	i (s)	j (s)	K (m)	L (s)	m (t)
Ib	9.15	9.03	8.06	7.70	7.23	6.94	$\frac{g_1}{4.54}$	$\frac{g_2}{3.89}$	3.91	3.47	2.51	1.53	1.23	0.85

Table 6. <sup>1</sup>H-NMR protons for Ic.

Comp	a (d)	B (d)	C (d)	d (d)	e (t)		f (t)	g (s)	h (s)	i (m)	j (s)	k (t)
Ic	9.34	8.00	7.44	7.37	$\frac{e_1}{4.55}$	$\frac{e_2}{4.13}$	4.23	3.40	2.82	2.63	1.71	0.85

**Elemental Analysis:** Table 7 indicated that the experimental values of the prepared ILs are in acceptable agreement with the theoretically calculated values.

Table 7. Elemental analysis of Ia, Ib & Ic.

Comp.	Elements							
	C%		H%		N%		Br %	
	Calc.	Obs.	Calc.	Obs.	Calc.	Obs.	Calc.	Obs.
Ia	56.55	56.60	8.26	8.31	7.33	7.37	27.87	27.91
Ib	57.24	57.27	8.41	8.45	7.15	7.18	27.20	27.25
Ic	57.24	57.03	8.41	8.54	7.15	7.26	27.20	27.17

**Thermo-gravimetric Analysis (TGA) and DTG** composite pictures of Ia, Ib, and Ic recorded high onset temperatures, which related to the resistance of these materials toward thermal degradation. Figure 6 confirmed that Ia, Ib, and Ic are thermally stable, and the actual first steps of decomposition were recorded as 247, 223, and 239 °C, respectively, while the final decomposition was up to 600 °C, which presented endothermal phenomena until reaching the maximum mass loss percent (100% wt. loss of the sample) [26]. The position of the methyl group affects the thermal stability; in the meta position (Ic), the compound showed higher thermal stability than in the para position (Ib) because of the effect of mesomeric resonance, which prevents C-bond leakage [27].

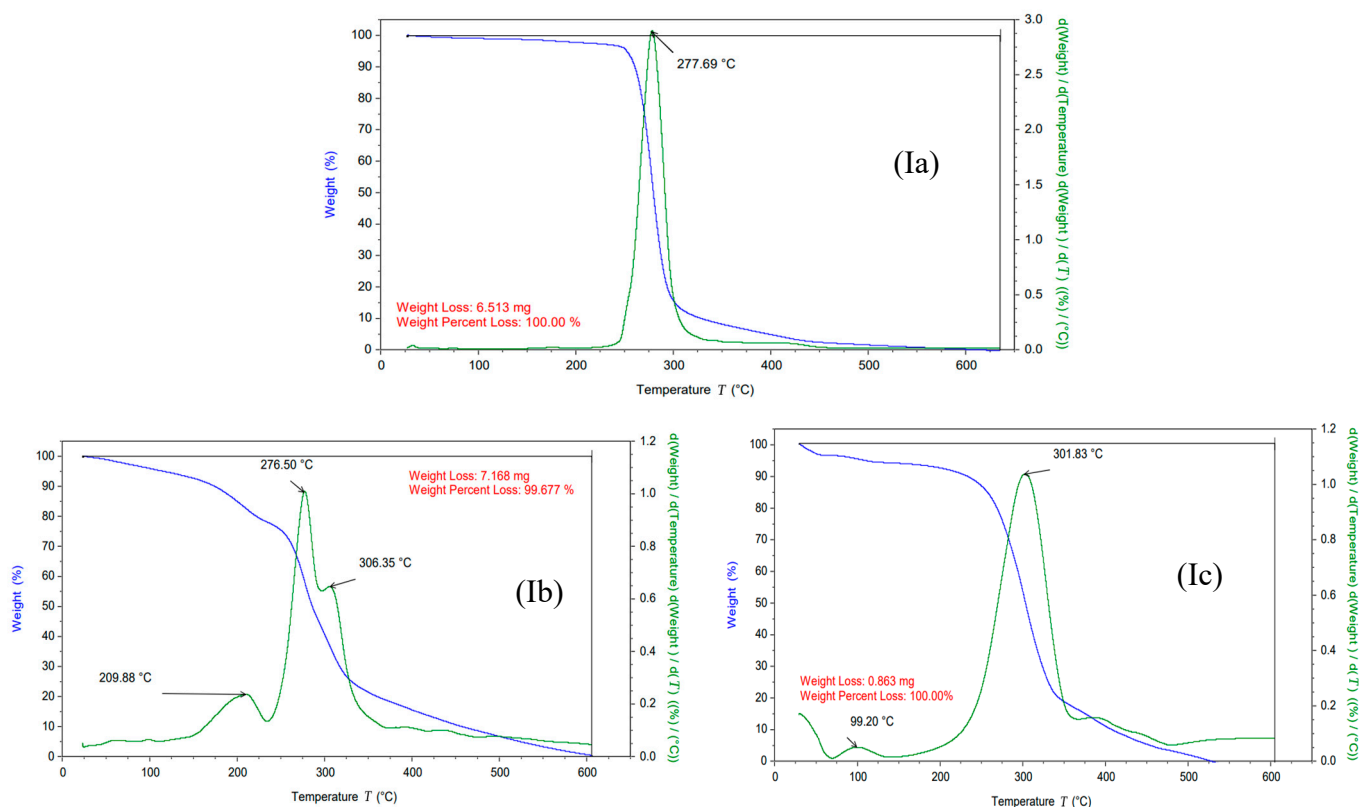


**Figure 6.** Thermal gravimetric Analysis of Ia, Ib & Ic.

### 3.2. Surface and Physical Characteristics of ILs

#### 3.2.1. Surface Tension and Critical Micelle Concentration (CMC)

The critical micelle concentrations (CMC) of Ia, Ib, and Ic were determined at 25 °C, as shown in Figure 7. The synthesized compounds' CMC has a low value and significant surface activity, as can be observed. Table 8 displays their CMC and surface tensions at CMCs. The adsorption of the synthesized compounds was studied using surface tension measurements. These results demonstrated a decrease in surface tension, indicating a high effect on surface activity. The results revealed that Ia, Ib, and Ic have significant power to lower aqueous system surface tension [21,28].

**Table 8.** Surface parameters of the synthesized ILs.

ILs	CMC mol/L	$\gamma_{CMC}$ mN/m	$\pi_{CMC}$ mN/m	$P_{C20}$	$\Gamma_{max} \times 10^{11}$ mol/cm <sup>2</sup>	$A_{min}$ nm <sup>2</sup>	$\Delta G^{\circ}_{mic}$ KJ/mol	$\Delta G^{\circ}_{ads}$ KJ/mol
Ia	$2.5 \times 10^{-3}$	33	39	$5.5 \times 10^{-6}$	2.921	56.840	−14.847	−28.199
Ib	$1.6 \times 10^{-3}$	32	40	$2.5 \times 10^{-6}$	4.286	38.738	−15.953	−23.886
Ic	$1.0 \times 10^{-3}$	34	38	$6 \times 10^{-5}$	8.050	20.633	−17.118	−21.840



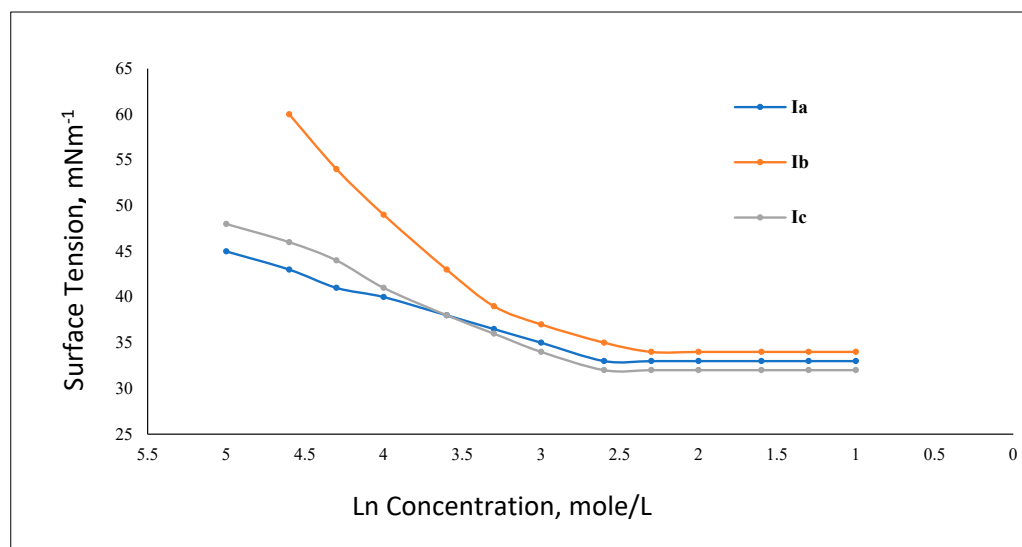


Figure 7. Surface tension isotherm of Ia, Ib & Ic.

It is well known that the intermolecular interactions of monomeric surfactants and their interactions with solvents primarily regulate the aggregation behavior of typical monocationic surfactants in solution. In contrast to conventional monocationic surfactants, dicationic surfactants' aggregation behavior in solution is governed by the cooperativeness of both intra- and inter-molecular contacts, in addition to their interactions with solvents.

The dicationic IL molecules must arrange the conformation in an aggregate state when the conformation is found in the free state. In this case, the two alkyl chains are as close as possible, and the spacer is gradually incorporated into the aggregate hydrophobic core as the spacer's hydrophobicity increases.

Additionally, in the aqueous solutions of dicationic ILs, the spacer causes a strong inclination to form a wide range of aggregate forms [21], such as worm-like micelles and tubule aggregates. An acceptable explanation for the development of worm-like micelles could be found in the surfactant packing parameter theory (SPP). By comparing monocationic with dicationic ILs as surfactants, it was found that they typically have higher SPP values, which causes the spontaneous formation of rod- or worm-shaped micellar aggregates even just above the CMC [29].

With the addition of the surfactant, the surface tension below the CMC was reduced. The surface tension was in the order  $Ic > Ia > Ib$ , while the CMC was in the order  $Ia > Ib > Ic$ . CMC is useful since it displays surfactant assembly proclivity in water. The micellization is driven by hydrophobic forces opposing electrostatic repulsion among the ionic head groups at the micelle surface. Micelles are known to be disorganized assemblies with a mobile hydrocarbon chain within. The Ic has a methyl group at position 3 of the pyridine ring, making it the most reactive. Micelles are generated by zwitter-ionic species with a characteristic nucleophilic group covalently connected to their portions [30].

The working action mechanism of cationic surfactants mainly depends on the adsorption of hydrophilic groups, which are represented by positively charged nitrogen atoms in Ia, Ib, and Ic, onto a polar hydrophobic group on a nonpolar phase. At lower concentrations, a higher  $\pi C_{20}$  represents a 20 mN/m decrease in surface tension. The low value of  $\pi CMC$  is directly related to the low surface activity. As shown in Table 8,  $\pi CMC$  varies between 40 and 38 dyne/cm. According to Gibb's adsorption isotherm, the relation between the surface tension and logarithmic concentration below the CMC region was used to calculate the surfactant molecules that adsorbed at the surface (max).

$$\Gamma_{max} = -(\delta\gamma/\delta \log c)_T/2.303RT \tag{7}$$

The IL solution concentration affects the number of ionic species ( $n$ ). If the surfactant is present near or on the surface, it will decrease the surface energy. By increasing the ILs' activity, the surface tension will decrease, and the maximum will be positive, as shown in Table 8.  $A_{\min}$  was recorded for Ic and could be calculated according to the following Equation (8):

$$A_{\min} = 10^{16}/N \cdot \Gamma_{\max} \quad (8)$$

where  $N$ , represent an Avogadro number.

### 3.2.2. Thermodynamics of Micellization and Adsorption

$\Delta G^{\circ}_{\text{mic}}$  provides details about the aggregation process nature gives information about the nature of the aggregation process. The following equation illustrates the gemini surfactant's energy as shown:

$$\Delta G^{\circ}_{\text{mic}} = -2.303RT \log(\text{CMC}) \quad (9)$$

Negative values of  $\Delta G^{\circ}_{\text{mic}}$  indicate that the process of micellization is spontaneous. Thermodynamic quantities relevant to micellization are the changes of free energy.

At ambient temperature and atmospheric pressure, the values of  $\Delta G^{\circ}_{\text{mic}}$  are always negative. The thermodynamic behavior of micellization was found, as Ic is less negative than Ib and Ia. The free energy of adsorption at the air-liquid interface (a measure of the free energy of transfer per mole of surfactant at a unit concentration from bulk to surface at unit pressure) was calculated using Equation (10):

$$\Delta G^{\circ}_{\text{ads}} = \Delta G^{\circ}_{\text{mic}} - (0.6023 \times 10^{-1} \times \pi_{\text{cmc}} \times A_{\min}) \quad (10)$$

A negative value of  $\Delta G^{\circ}_{\text{ads}}$  indicates that the adsorption process is spontaneous. Furthermore, the higher values of  $\Delta G^{\circ}_{\text{ads}}$  compared to  $\Delta G^{\circ}_{\text{mic}}$ , Table 8 show more spontaneous adsorption at the solution-to-air interface than micellization does in the bulk.

### 3.3. Quantum Chemical Calculations

The optimized geometry and the frontier molecular orbital density of the investigated compounds are shown in S1. The chemical reactivity of the prepared compounds was explained by the value of  $\Delta E$ . Molecules that have a small ( $\Delta E$ ) are less stable and more reactive. ( $\sigma$ ) and ( $\eta$ ) are properties that are related to the reactivity of the compounds. Small ( $\sigma$ ) values correspond to soft molecules that can easily donate electrons to the acceptor system.

Consequently, adsorption on asphaltene surfaces could take place easily for the molecule that has the highest ( $\sigma$ ) value, postponing the asphaltene dispersion. ( $\mu$ ) is another index factor that can illustrate the effect of prepared compounds on asphaltenes, which can be defined as the measurements of the bond polarity in molecule S2. According to ( $\sigma$ ) and ( $\eta$ ) values, the studied compounds were considered soft molecules.

The results in Table 9 indicate that Ia, Ib, a Ic have an appreciable ( $\mu$ ) that facilitates the interaction with asphaltene [31]. Data showed that Ic is the most effective dispersant that is compatible with (A) (1.119 eV) due to its high electron density and high aromaticity, which accelerate the penetration of crude oil and accelerate the adsorption on asphaltene surfaces and their aggregation.

**Table 9.** Quantum chemical calculations for Ia, Ib & Ic.

ILs	$E_{\text{HOMO}}$ (eV)	$E_{\text{LUMO}}$ (eV)	$\Delta E$ (eV)	Ionization Potential I (eV)	Electron Affinity A (eV)	Dipole Moment $\mu$ (Debye)	Electronegativity ( $\text{eV mol}^{-1}$ )	Hardness ( $\eta$ ) ( $\text{eV mol}^{-1}$ )	Softness $\text{eV}^{-1}$
Ia	−1.542	−1.230	0.312	1.542	1.230	52.4894	1.386	0.156	6.4102564
Ib	−1.395	−0.930	0.465	1.395	0.930	49.0859	1.1625	0.2325	4.3010753
Ic	−1.219	−1.119	0.100	1.219	1.119	49.2601	1.169	0.05	20

### 3.4. Evaluation of the Synthesized ILs as Oil Dispersants:

The evaluation of the synthesized compounds as dispersants was discussed using different ratios of dispersants to crude oil, wt.% (DOR), at specific temperatures (10 and 30 °C).

#### 3.4.1. Effect of Temperatures

It was noticed that the dispersion efficiency of three newly synthesized compounds increased with increasing temperature for the same dispersant. In the case of cold sea water, Table 10 (at 10 °C) shows that Ia, Ib, and Ic recorded 5.32, 20.45, and 33.61% as dispersion efficiency, respectively. Whereas, the dispersion efficiency increased in warm water (30 °C), which recorded 12.28, 52.55, and 66.80% for Ia, Ib, and Ic in order. Whereas, the dispersion efficiency increased in warm water (30 °C), which recorded 12.28, 52.55, and 66.80% for Ia, Ib, and Ic in order in Table 11.

**Table 10.** Dispersion efficiency % @ 10 °C.

Comp.	Dispersion Efficiency % at 10 °C			
	(Dispersant: Crude Oil) wt.%			
	(0.4:10)	(0.8:10)	(1.2:10)	(1.6:10)
Ia	2.49	5.32	4.02	3.88
Ib	16.88	20.45	18.54	17.82
Ic	13.47	33.61	23.61	11.57

**Table 11.** Dispersion efficiency % @ 30 °C.

Comp.	Dispersion Efficiency % at 30 °C			
	(Dispersant: Crude Oil) wt.%			
	(0.4:10)	(0.8:10)	(1.2:10)	(1.6:10)
Ia	6.40	12.28	9.48	7.91
Ib	20.65	52.55	28.88	27.75
Ic	21.90	66.80	61.08	54.32

#### 3.4.2. Effect of DOR

Tables 10 and 11 indicated that the efficiency of the synthesized dispersants increased with increasing the DOR, wt.%, from (0.4:10) to (0.8:10), started slightly by using (1.2:10), and decreased again when (1.6:10) was used. So, the optimum ratio in this study was 0.8:10.

#### 3.4.3. Effect of Cation Structure

Three derivatives of pyridine were used: pyridine, 3-methylpyridine, and 4-methylpyridine, and the results showed that the dispersion efficiency ranked as Ia < Ib < Ic which refers to the presence of CH<sub>3</sub> as an electron-releasing group at position 4, which activates the pyridinium ring more than in position 3 Figure 8. In para-position, the hyper conjugation of the methyl group adjacent to the pyridine ring increases the electron density of N, so the effects of the N atom increase.

The amphiphilic ILs might be completely absorbed on the surface of the oil droplet, and the dispersion efficiency increases due to the decrease in oil–water interfacial tension, which facilitates the formation of small droplets in large quantities to be entered through the water column, resulting in an emulsion that seems to have a sun-like structure. The presence of non-polar ends in the synthesized ILs would help to form a stable emulsion via van der Waals forces [32,33]. Increasing the IL concentrations results in an increase in the IL molecules adsorbed at the oil–water interface. According to the nature of IL molecules, they provide electrostatic and steric barriers to the coalescence of the dispersed oil drops.

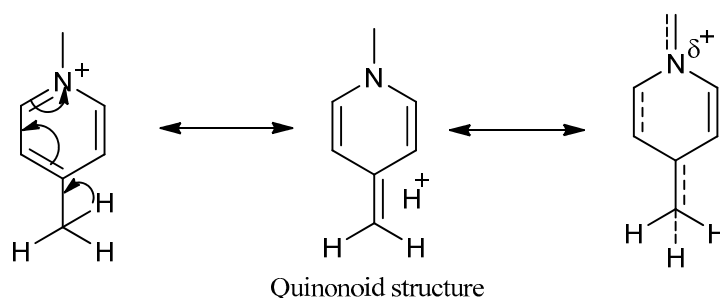


**Figure 8.** Hyper conjugation of 4-methyl pyridine.

### 3.5. Stability of Crude Oil & Water Emulsions

In order to evaluate the performance of the prepared samples as oil spill dispersants regarding benchmark industrial standards, samples of crude oil and water were emulsified by Tween-80 (as a commercial oil spill dispersant) [34], Ia, Ib, and Ic, to evaluate the emulsion stability at 30 °C with (0.8:10 wt.%) DOR. Sample photos were taken immediately after sample preparation (at 0 min) and after 30 min. The results are shown in Figure 9. Firstly, all samples formed a completely homogenous emulsion. Consequently, the prepared emulsion with Tween-80 separated into two clear layers after 30 min. The upper, darker layer is oil-rich, while the lower layer is water-rich and lighter in color. The formed emulsions with Ia, Ib, and Ic were gradually stable, and Ic showed the most stability due to the highest dispersion and emulsification capacity compared to others.

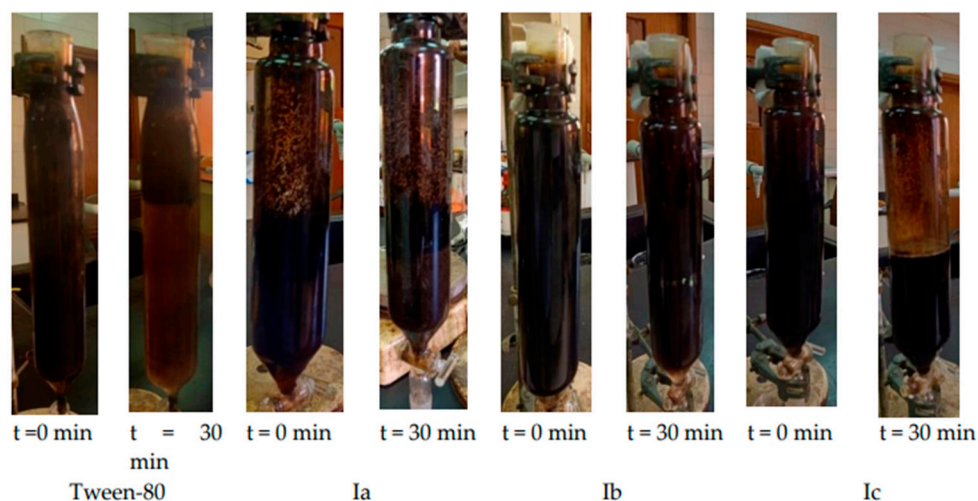


**Figure 9.** Stability of crude oil & water emulsion.

### 3.6. Group Composition of Undispersed Crude Oil

The treated crude oil with the different synthesized dispersants at 30 °C with the optimum ratio (0.8–10) wt.% was recovered, weighted accurately, and separated into its components via SARA analysis. Gravimetrically, the dispersion efficiency was determined as shown in Table 12.

**Table 12.** Gravimetric determination of efficiency.

IL Dispersants	% of Dispersed Crude Oil	% of Undispersed Crude Oil
Ia	12.08	87.92
Ib	53.17	46.83
Ic	67.01	32.99

All results obtained through gravimetric and UV spectroscopy for efficiency determination led to the same trend with accepted values.

Results revealed that the higher asphaltene and resin content is directly proportional to the dispersion [35]. The highest percentage of asphaltene and resin was recorded in dispersant Ic Table 13.

**Table 13.** SARA analysis of treated crude oil.

Chemical Composition, %				
	Asphaltene	Maltene, wt.%		
		Oil, wt.%		
		Resin	Saturate	Aromatic
Ia	25.08	31.99	13.24	29.69
Ib	29.74	41.45	9.01	19.80
Ic	32.45	43.42	6.45	17.68

### 3.6.1. Gas Chromatography Analysis of Saturates Fraction

The dispersion efficiency was also understood by studying the alkane’s distributions (Figure 10). It was noticed that the gas chromatograph of crude oil is considered a fingerprint to be compared with the treated crude oil using Ia, Ib, and Ic. Clearly, it was found that there is a change in GC profiles; otherwise, there is a reduction in peak heights or disappearance of the number of paraffin peaks. Undispersed, treated crude oil with Ic dispersant recorded the highest reduction.

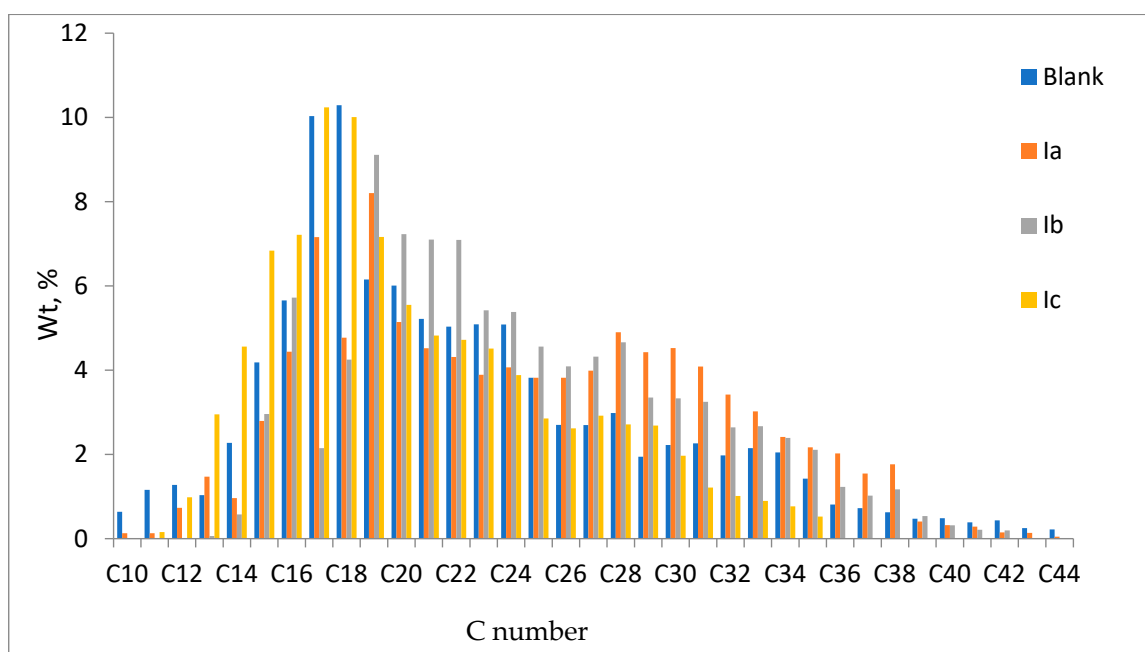


**Figure 10.** C number of blank and treated crude oil with Ia, Ib & Ic.

### 3.6.2. HPLC for Polyaromatic Hydrocarbons (PAHs)

Figure 11 illustrates the PAH fingerprints of the studied (blank) and treated crude oils via Ia, Ib, and Ic [36]. PAHs were characterized by the formation of high-molecular-weight aromatic rings (di-, tri-, tetra-, penta-, and hexa-). The presence of aromatics with high molecular weight aromatic rings (tetra-, penta-, and hexa-) is more carcinogenic than that of those of smaller molecular weight (di and tri). The disappearance of higher PAHs in undispersed, treated crude oil is referred to as the degradation of them as an effect of dispersion. HPLC results showed that the efficiency of dispersants’ effect on PAH distribution increased, whereas penta and hexa aromatics (carcinogenic parts) decreased.

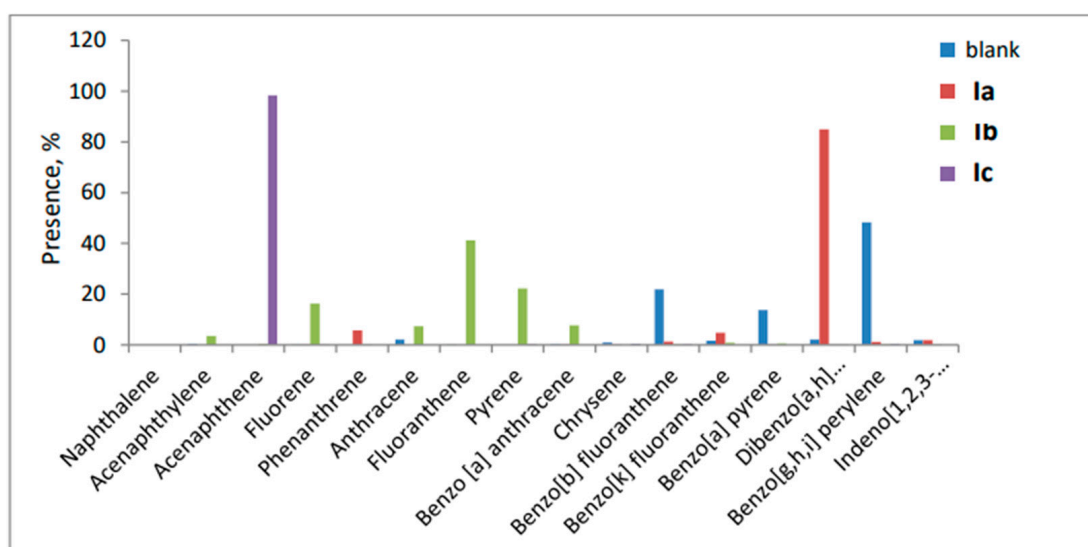


**Figure 11.** PAHs of blank and treated crude oil with Ia, Ib & Ic.

### 3.7. Acute Toxicity of the Prepared Dispersants

The toxicity of Ia, Ib, and Ic was tested to evaluate their toxicity against fish (Nile tilapia and *Oreochromis niloticus*). Results indicated an acute fish toxicity test (LC50) of concentrations greater than 100 ppm after 96 h of observation. These values indicate that the LC50s of Ia, Ib, and Ic record 13.25, 17.75, and 37.5 mg/L, respectively, which are located between 10 and 100 mg/L [32], providing that the synthesized dispersants are “slightly toxic” under the acute toxicity test. By comparing the LC50 of the prepared ILs with that of commercial Corexit 9500 (96 h LC50 = 35.9 mg/L), it was found that the synthesized dispersants were less toxic. The results of the toxicity test and assessment of ILs against marine toxicity confirmed the ability to use the synthesized ILs as potential dispersants and safety applications for oil remediation with a slight toxicity effect on the marine ecosystem [37].

## 4. Conclusions

In the presented work, a series of dicationic ionic liquids (Ia, Ib, and Ic) were synthesized with different pyridine derivatives and well characterized via FT-IR, <sup>1</sup>H-NMR, and elemental analysis. They recorded good physico-chemical properties (surface activity and thermal stability). Density functional theory (DFT) parameters were studied to investigate the geometry optimization of electronic structures, energy gap ( $\Delta E$ ), reactivity, hardness, and softness. The calculated parameters showed that Ic is the most effective dispersant; due to its high electron density and high aromaticity, it accelerates the penetration of crude oil, the adsorption on asphalt surfaces, and its aggregation.

The evaluation of Ia, Ib, and Ic as oil spill dispersants occurred by spectroscopic (U.V. spectroscopy) and gravimetric techniques at different temperatures (10 and 30 °C). The experimental data showed that the synthesized ILs ranked as Ia < Ib < Ic which refer to the presence of the electron-releasing group (CH<sub>3</sub>) at position 4, activating the pyridinium ring more than in position 3. Dispersion efficiency increased with increasing the ratio of dispersant to crude oil; the optimum ratio of dispersants to crude oil (DOR) in this study was (0.8:10) wt.% and recorded 33.61% at 10 °C and 66.0% at 30 °C. Undispersed, treated crude oil with dispersants was studied via GC and HPLC techniques. The results showed that the dispersants affected saturated and PAH distributions.

The toxicity of Ia, Ib, and Ic was tested to evaluate their toxicity against fish, and the studies indicated that they are “slightly toxic” under the acute toxicity test (LC50 between 10 and 100 mg/L). Generally, the excellent oil spill dispersion and slight toxicity of the newly synthesized ILs could provide a real chance to be applied in industrial oil spill remediation.

**Author Contributions:** Conceptualization, Y.M.M., M.I.N., R.I.A. and R.A.E.-N.; methodology, R.A.E.-N., M.W., C.E.E.S. and D.A.I.; software, R.A.E.-N.; validation, M.I.N. and R.A.E.-N.; formal analysis, R.A.E.-N. and C.E.E.S.; investigation, R.A.E.-N. and C.E.E.S.; resources, R.A.E.-N.; writing—original draft preparation, R.D.A., R.A.E.-N. and C.E.E.S.; writing—review, M.M.H.K., Y.M.M., M.I.N., R.I.A. and R.A.E.-N.; funding acquisition, R.D.A.; editing, R.A.E.-N.; supervision, M.I.N., R.I.A., Y.M.M. and M.M.H.K. All authors have read and agreed to the published version of the manuscript.

**Funding:** This research work was funded by Institutional Fund Projects under grant No. (IFPIP: 487-665-1443). The authors gratefully acknowledge the technical and financial support provided by the Ministry of Education and King Abdulaziz University, DSR, Jeddah, Saudi Arabia.

**Conflicts of Interest:** The authors declare no conflict of interest.

## References

1. Li, P.; Cai, Q.; Lin, W.; Chen, B.; Zhang, B. Offshore oil spill response practices and emerging challenges. *Mar. Pollut. Bull.* **2016**, *110*, 6–27. [[CrossRef](#)]
2. Burrows, P.; Rowley, C.K.; Owen, D. Torrey 711 canyon: A case study in accidental pollution. *Scott. J. Political Econ.* **1974**, *21*, 237–258. [[CrossRef](#)]
3. Brakstad, O.G.; Lewis, A.; Beegle-Krause, C.J. A critical review of marine snow in the context of oil spills and oil spill dispersant treatment with focus on the Deepwater Horizon oil spill. *Mar. Pollut. Bull.* **2018**, *135*, 346–356. [[CrossRef](#)] [[PubMed](#)]
4. Nissanka, I.D.; Yapa, P.D. Calculation of oil droplet size distribution in ocean oil spills: A review. *Mar. Pollut. Bull.* **2018**, *135*, 723–734. [[CrossRef](#)]
5. Chen, J.; Zhang, W.; Li, S.; Zhang, F.; Zhu, Y.; Huang, X. Identifying critical factors of oil spill in the tanker shipping industry worldwide. *J. Clean. Prod.* **2017**, *180*, 1–10. [[CrossRef](#)]
6. Johannsdottir, L.; Cook, D. Systemic risk of maritime-related oil spills viewed from an Arctic and insurance perspective. *Ocean Coast. Manag.* **2019**, *179*, 104853. [[CrossRef](#)]
7. Cirer-costa, J.C. Tourism and its hypersensitivity to oil spills. *Mar. Pollut. Bull.* **2015**, *91*, 65–72. [[CrossRef](#)]
8. Nelson, J.R.; Grubestic, T.H.; Sim, L.; Rose, K. A geospatial evaluation of oil spill impact potential on coastal tourism in the Gulf of Mexico. *Comput. Environ. Urban Syst.* **2018**, *68*, 26–36. [[CrossRef](#)]
9. Hoof, L.V.; Den Burg, S.W.; Banach, J.L.; Rockmann, C.; Goossen, M. Can multi-use of the sea be safe? A framework for risk assessment of multi-use at sea. *Ocean Coast. Manag.* **2020**, *184*, 105030. [[CrossRef](#)]
10. Shah, M.H.; Reddy, A.V.B.; Yusup, S.; Goto, M.; Moniruzzaman, M. Ionic liquid-biosurfactant blends as effective dispersants for oil spills: Effect of carbon chain length and degree of saturation. *Environ. Pollut.* **2021**, *284*, 117–119.
11. Shah, M.H.; Reddy, A.V.B.; Moniruzzaman, M. Ionic liquid-based surfactants for oil spill remediation. In *Ionic Liquid-Based Technologies for Environmental Sustainability*; Elsevier: Amsterdam, The Netherlands, 2022; ISBN 9780128245453.
12. Azubuike, C.C.; Chikere, C.B.; Okpokwasili, G.C. Bioremediation techniques—classification based on site of application: Principles, advantages, limitations and prospects. *World J. Microbiol. Biotechnol.* **2016**, *32*, 180. [[CrossRef](#)]
13. Gong, Y.; Zhao, X.; O'Reilly, S.E.; Qian, T.; Zhao, D. Effects of oil dispersant and oil on sorption and desorption of phenanthrene with Gulf Coast marine sediments. *Environ. Pollut.* **2014**, *185*, 240–249. [[CrossRef](#)]
14. Nabipour, M.; Ayatollahi, S.; Keshavarz, P. Application of different novel and newly designed commercial ionic liquids and surfactants for more oil recovery from an Iranian oil field. *J. Mol. Liq.* **2017**, *230*, 579–588. [[CrossRef](#)]
15. Santos, J.M., Jr.; Wisniewski, A.; Eberlin, M.N.; Schrader, W. Comparing crude oils with different API Gravities on a molecular level using mass spectrometric analysis—Part 1: Whole Crude Oil. *Energies* **2018**, *11*, 2766. [[CrossRef](#)]
16. Adawiyah, N.; Moniruzzaman, M.; Hawatulaila, S.; Goto, M. Ionic liquids as a potential tool for drug delivery systems. *Med. Chem. Commun.* **2016**, *7*, 1881–1897. [[CrossRef](#)]
17. Lotfi, M.; Moniruzzamana, M.; Sivapragasam, M.; Kandasamy, S.; Mutalib, M.I.A.; Alitheen, N.B.; Gotode, M. Solubility of acyclovir in nontoxic and biodegradable ionic liquids: COSMO-RS prediction and experimental verification. *J. Mol. Liq.* **2017**, *243*, 124–131. [[CrossRef](#)]
18. Moniruzzaman, M.; Ono, T. Separation and characterization of cellulose fibers from cypress wood treated with ionic liquid prior to laccase treatment. *Bioresour. Technol.* **2013**, *127*, 132–137. [[CrossRef](#)]
19. Mustahil, N.A.; Baharuddin, S.H.; Abdullah, A.A.; Reddy, A.V.B.; Mutalib, M.I.A.; Moniruzzaman, M. Synthesis, characterization, ecotoxicity and biodegradability evaluations of novel biocompatible surface active lauroyl sarcosinate ionic liquids. *Chemosphere* **2019**, *229*, 349–357. [[CrossRef](#)] [[PubMed](#)]
20. El-Nagar, R.A.; Ghanem, A.A.; Nessim, M.I. Capture of CO<sub>2</sub> from Natural Gas Using Ionic Liquids. In *Shale Gas-New Aspects and Technologies*; IntechOpen: London, UK, 2018; ISBN 978-1-78923-618-7.
21. El shafiee, C.E.; El Nagar, R.A.; Nessim, M.I.; Khalil, M.M.H.; Shaban, M.E.; Alharthy, R.D.; Aismail, D.; Abdallah, R.I.; Moustafa, Y.M. Application of asymmetric dicationic ionic liquids for oil spill remediation in sea water. *Arab. J. Chem.* **2021**, *14*, 103123. [[CrossRef](#)]

22. El-Nagar, R.A.; Nessim, M.; El-Wahab, A.A.; Ibrahim, R.; Faramawy, S. Investigating the efficiency of newly prepared imidazolium ionic liquids for carbon dioxide removal from natural gas. *J. Mol. Liquids* **2017**, *237*, 484–489. [[CrossRef](#)]
23. Dost, K.; Ideli, C. Determination of polycyclic aromatic hydrocarbons in edible oils and barbecued food by HPLC/UV-Vis detection. *Food Chem.* **2012**, *133*, 193–199. [[CrossRef](#)]
24. Zhang, J.; Cheng, C.; Lu, C.; Li, W.; Li, B.; Wang, J.; Wang, J.; Du, Z.; Zhu, L. Comparison of the toxic effects of non-task-specific and task-specific ionic liquids on zebrafish. *Chemosphere* **2022**, *294*, 133643. [[CrossRef](#)]
25. Brycki, B.; Metecka, I.; Kozirog, A.; Otlewska, A. Synthesis, structure and antimicrobial properties of novel benzalkonium chloride analogues with pyridine rings. *Molecules* **2017**, *22*, 130. [[CrossRef](#)] [[PubMed](#)]
26. Yu, J.; Wheelhouse, R.T.; Honey, M.A.; Karodia, N. Synthesis and characterisation of novel nopyl-derived phosphonium ionic liquids. *J. Mol. Liq.* **2020**, *316*, 113857. [[CrossRef](#)]
27. Muhammad, N.; Gao, Y.; Iqbal, F.; Ahmad, P.; Ge, R.; Nishan, U.; Rahim, A.; Gonfa, G.; Ullah, Z. Extraction of biocompatible hydroxyapatite from fish scales using novel approach of ionic liquid pretreatment. *Sep. Purif. Technol.* **2016**, *161*, 129–135. [[CrossRef](#)]
28. Nakahara, H.; Nishino, A.; Tanaka, A.; Fujita, Y.; Shibata, O. Interfacial behavior of gemini surfactants with different spacer lengths in aqueous medium. *Colloid Polym. Sci.* **2019**, *297*, 183–189. [[CrossRef](#)]
29. Baoli, S. The strengths of van der Waals and electrostatic forces in 1-alkyl-3-methylimidazolium ionic liquids obtained through Lifshitz theory and Coulomb formula. *J. Mol. Liq.* **2020**, *320*, 114412.
30. Ahmed, S.M.; Khidr, T.T.; Ismail, D.A. Effect of gemini surfactant additives on pour point depressant of crude oil. *J. Dispers. Sci. Technol.* **2018**, *39*, 1160–1164. [[CrossRef](#)]
31. Ghanem, A.; Alharthy, R.D.; Desouky, S.M.; El-Nagar, R.A. Synthesis and Characterization of Imidazolium-Based Ionic Liquids and Evaluating Their Performance as Asphaltene Dispersants. *Materials* **2022**, *15*, 1600. [[CrossRef](#)]
32. Baharuddin, S.H.; Mustahil, N.A.; Reddy, A.V.B.; Abdullah, A.A.; Mutalib, M.I.A.; Moniruzzaman, M. Development, formulation and optimization of a novel biocompatible ionic liquids dispersant for the effective oil spill remediation. *Chemosphere* **2020**, *249*, 126125. [[CrossRef](#)]
33. Jin, J.; Wang, H.; Jing, Y.; Liu, M.; Wang, D.; Li, Y.; Bao, M. An Efficient and environmental-friendly dispersant based on the synergy of amphiphilic surfactants for oil spill remediation. *Chemosphere* **2018**, *215*, 241–247. [[CrossRef](#)] [[PubMed](#)]
34. Mansoor, M.; Shah, U.H.; Yahya, W.Z.N.; Goto, M.; Moniruzzaman, M. Surface active ionic liquid and Tween-80 blend as an effective dispersant for crude oil spill remediation. *Environ. Technol. Innov.* **2021**, *24*, 101868.
35. Ashoori, S.; Sharifi, M.; Masoumi, M.; Salehi, M.M. The relationship between SARA fractions and crude oil stability. *Egypt. J. Pet.* **2017**, *26*, 209–213. [[CrossRef](#)]
36. Driskell, W.B.; Payne, J.R. Macondo oil in northern Gulf of Mexico waters—Part 2: Dispersant-accelerated PAH dissolution in the Deepwater Horizon plume. *Mar. Pollut. Bulletin* **2018**, *129*, 412–419. [[CrossRef](#)] [[PubMed](#)]
37. Pie, H.V.; Mitchelmore, C.L. Acute toxicity of current and alternative oil spill chemical dispersants to early life stage blue crabs (*Callinectes sapidus*). *Chemosphere* **2015**, *128*, 14–20. [[CrossRef](#)]

**Disclaimer/Publisher's Note:** The statements, opinions and data contained in all publications are solely those of the individual author(s) and contributor(s) and not of MDPI and/or the editor(s). MDPI and/or the editor(s) disclaim responsibility for any injury to people or property resulting from any ideas, methods, instructions or products referred to in the content.